Prediction of NOx emissions and pathways in premixed ammonia-hydrogen-air combustion using CFD-CRN methodology

Shivansh Chaturvedi [1], R. Santhosh [1, *], Syed Mashruk [2], Rajneesh Yadav [1], and Agustin Valera-Medina [2]

[1] Department of Mechanical Engineering, Indian Institute of Technology (BHU) Varanasi, Varanasi 221005, Uttar Pradesh, India

[2] College of Physical Sciences and Engineering, Cardiff University, Queen's Building, Cardiff CF24 3AA, UK

* Corresponding author: E-mail address: rsanthosh.mec@iitbhu.ac.in (R. Santhosh)

Abstract

Ammonia-hydrogen blends have gained significance as they are carbon-free energy-dense fuels. However, NO_x emissions have been a significant concern. In this study, the emissions from the premixed combustion of $70/30_{VOL.\%}$ NH_3/H_2 blend is studied using the computational fluid dynamics (CFD)- chemical reactor network (CRN) approach. The velocity, temperature, and species field are first obtained using CFD, based on which, a network consisting of perfectly stirred reactors (PSR) and plug flow reactor (PFR) is constructed. Three mechanisms have been implemented in the CRN to predict the NO and N_2O emissions. It is shown that the trend of NOx is correctly predicted by the CRN over a wide range of equivalence ratios (ϕ) of 0.65-1.2 as compared to the authors' recently published experimental data. It is demonstrated that a single CRN (based on the CFD for a specific ϕ) can be run to cover the range of ϕ = 0.65 to 1.2 by scaling the temperature input to each reactor of the CRN. To contrast the NO pathways at different ϕ, quantitative reaction pathway diagrams (QRPD) are constructed, and dominant production and consumption pathways of NO for lean and rich combustion are established. The shifts in reaction pathways with ϕ are noted and found to be governed by OH, O, and H radicals. Next, the effect of stoichiometry on these radicals is established. Finally, the experimental trend of high NO close to stoichiometric combustion and high N_2O in very lean combustion along with their respective pathways are explained.

Keywords: Ammonia**,** Hydrogen, CFD-CRN, Emissions, NO_x, Reaction Pathways

1. Introduction

In the present era, the most prominent problem is the fast depletion of hydrocarbon fuels and the pollution generated by hydrocarbon fuels, especially greenhouse gases such as carbon dioxide [1]. Renewable energy resources can play an important role in minimizing the usage of hydrocarbon fuel. Because of low capacity and intermittency in power generation through renewable resources, it is necessary to explore other options for energy storage, and chemical energy storage in the form of energy-dense fuels is one of the best options [2-4]. A promising alternative can be found in energy-dense fuels like hydrogen, ammonia, methane, and other cyclic hydrocarbon which can be stored in large quantities for the long run. Of these, hydrogen and ammonia are the only carbon-free alternatives [2].

Hydrogen can be considered the fuel of the future for energy generation as it contains 120 MJ/kg of energy [5]. Hydrogen can be generated by electrolysis of water via electricity generated by renewable energy resources in the form of green hydrogen [6, 7]. Due to low density and compressibility, it is very costly and dangerous to transport it through pipes [8]. Ammonia is a hydrogen-laden gas (contains 17.6% hydrogen by mass) and hence, acts as a hydrogen carrier. Green hydrogen can play an important role in the production of ammonia by the Haber–Bosch process using atmospheric nitrogen [9]. Ammonia has a higher volumetric energy density (10.8 MJ/L at 300 K and 8.6 bar), compared to hydrogen (7 MJ/L at 300 K and 10 bar). Since ammonia is used for the production of fertilizers, there exists a well-established transportation facility [10].

Because of its high octane number (~130) and low burning velocity (7 cm/s), ammonia is difficult to burn in existing internal combustion engines [12]. Attempts have been made to burn it in an I.C. engine with some modifications in compression ratio from 16:1 to 35:1 [13]. Gas turbine engines were also tested with pure ammonia and found that pure ammonia can be used to start the gas turbine engine. It is better to start with conventional fuel and then increase the mass fraction of ammonia from 0 to 100%. With a higher equivalence ratio (~1.2), because of excess ammonia, unburnt hydrogen remains inside the engine so a double-stage engine will be necessary in case of pure ammonia [14].

It is seen in the previous studies that 28% dissociation of ammonia exhibits similar characteristics as methane flame so there is ongoing research on different blends of ammonia and hydrogen [15]. In continuation to this research 50-50% [16], 60-40%, 70-30%, 80-20%, and 90-10% [17-18] blends of ammonia-hydrogen have already been studied experimentally and concluded that 70-30% and 80-20% blend are most stable as others are more prone to flash-back or blow-out. These blends are very sensitive to pressure and temperature. With an increase in temperature and pressure reactivity of flame decreases which leads to longer flame [19-20]. For the emission study, most of the research is done through experiments and only a few are related to the numerical study.

The blending of ammonia and hydrogen helps to overcome several practical problems associated with pure ammonia or pure hydrogen fuels, but the issue of high NO_x emissions must be addressed for such a blend. Some of the important studies on the reaction pathways of ammonia, involving the production and consumption of NO_x are discussed here. Lindstedt et al. [21] found NH_2 + O and NH + OH reactions to be important in ammonia flames. Further, NH_2 and N were found to be important for NO conversion. Skreiberg et al. [22] observed that the presence of NO promotes the path $NH_3 \rightarrow NH_2 \rightarrow N_2$ instead of $NH_3 \rightarrow NH_2 \rightarrow NH \rightarrow N$. Tian et al. [23] studied various ammonia-methane blends and reported $H + O_2 \rightarrow O + OH$, $NH_2 + O \rightarrow HNO + H$, $NH_2 + NO \rightarrow N_2 + H_2O$, and $NH + NO \rightarrow N_2O + H$ to be the most significant reactions in NO and N_2 conversions. Duynslaegher et al. [24] studied premixed ammonia-air mixtures in the context of IC engines and concluded that NO formation was majorly impacted by equivalence ratio, not temperature or compression ratio. Song et al. [25] studied ammonia combustion at high pressure and found NO to be formed from NH_3 majorly via HNO intermediate and NH_2 to be the major species in NO mitigation. In the same study, the highest sensitive reactions were found to be those that consumed NH_3 by producing OH. Otomo et al. [26] not only discussed the advantages of blending hydrogen and ammonia but also performed ROP analysis to discuss the H_2O consumption and regeneration pathways. Kobayashi et al. [27] discussed the kinetics of ammonia combustion in detail and concluded that NH_3 is majorly consumed with the help of OH and NH_i (i = 0, 1, 2) oxidise to NO, mainly through an HNO intermediate, or reduced NO, depending on availability of O/H radicals.

For the detailed analysis of reaction pathways as discussed above, the combustion is modelled using a chemical reactor network (CRN). In the present study, the construction of CRN is carried out using the hybrid CFD-CRN methodology. One of the first instances of developing CRN based on computational fluid dynamics (CFD) results is found in Sturgess and Shouse [28]. This procedure, which has come to be known as the CFD-CRN methodology, has been used extensively for the prediction of NO_x and CO emissions. Benedetto et al. [29] and Benedetto et al. [30] discussed the implementation of this tool in real combustion systems to predict emissions. Faravelli et al. [31] implemented a similar approach to industrial boilers and furnaces for determining NO_x formation. Falcitelli et al. [32] presented this approach as a process for the optimisation of the environmental performance of industrial combustors. Several studies like Novosselov et al. [33], Lebedev et al. [34], Park et al. [35], Nguyen et al [36], and Yousefian et al. [37] have used the CFD-CRN methodology for the prediction of emissions in gas turbine combustors. A similar analysis of emissions using the CFD-CRN methodology has been performed on the present 70/30 ammonia-hydrogen fuel blend in this study.

The present study aims to explain the trends of NO emissions against the equivalence ratio by implementing the hybrid CFD-CRN methodology. The CRNs in the present study are validated against the experimental results from one of the authors' previous works [38], where the 70/30 blend of ammonia/hydrogen by volume

is studied. As discussed above, this blend has been reported to provide a reasonable trade-off between the tendency of flashback in hydrogen-rich blends and blow-off stability in rich combustion. This blend has also been found to resemble widely used hydrocarbon fuels like methane and propane, in terms of flame speed, ignition energy, quenching distance, etc. [39] For this blend, the minimum ignition energy was found to be lower than that for propane-air (0.37 mJ) and was achieved across a wider range of equivalence ratios. The minimum quenching distance was found to be 2.1mm, close to that for propane-air (1.9mm). The flammability limits of this blend were also found to be close to that of methane-air. Therefore this study specifically focuses on the 70/30 blend of ammonia/hydrogen by volume.

This blend has been analysed using CRNs and three widely-used mechanisms in the literature have been comparatively studied, viz, Wang et al. mechanism [40], Nakamura et al. mechanism [41], and Glarborg mechanism [42], which have been found to closely predict the experimental data for the above-discussed blend [43]. The three mechanisms are compared to determine which mechanism(s) predict the NOx better for the considered blend. The differences and similarities between mechanisms have been noted at each step of the discussion. The best mechanism(s) identified are probed further to understand the pathways of NOx formation.

The trends and pathways reported in the experimental results [38] are explained using rates of production (ROP) analysis and quantitative reaction pathway diagrams (QRPD) from the first principles in this study. To the authors' best knowledge, the CFD-CRN methodology has not been applied in the context of ammonia-hydrogen blends and the present study is the first of its kind. The findings from this study aim to further the understanding of NOx and its pathways, which could open up new avenues in the establishment of ammonia-hydrogen as a widely applicable green alternative fuel. Further, this study also proves the validity of the CFD-CRN methodology for analysing ammonia-hydrogen blends with various reaction mechanisms. As evidenced by the accuracy of this methodology in this study, a relatively low-cost CFD-CRN can correctly predict the trend (and at some ϕ, very close values) as compared to expensive and time-consuming experiments.

2. Experimental Methodology

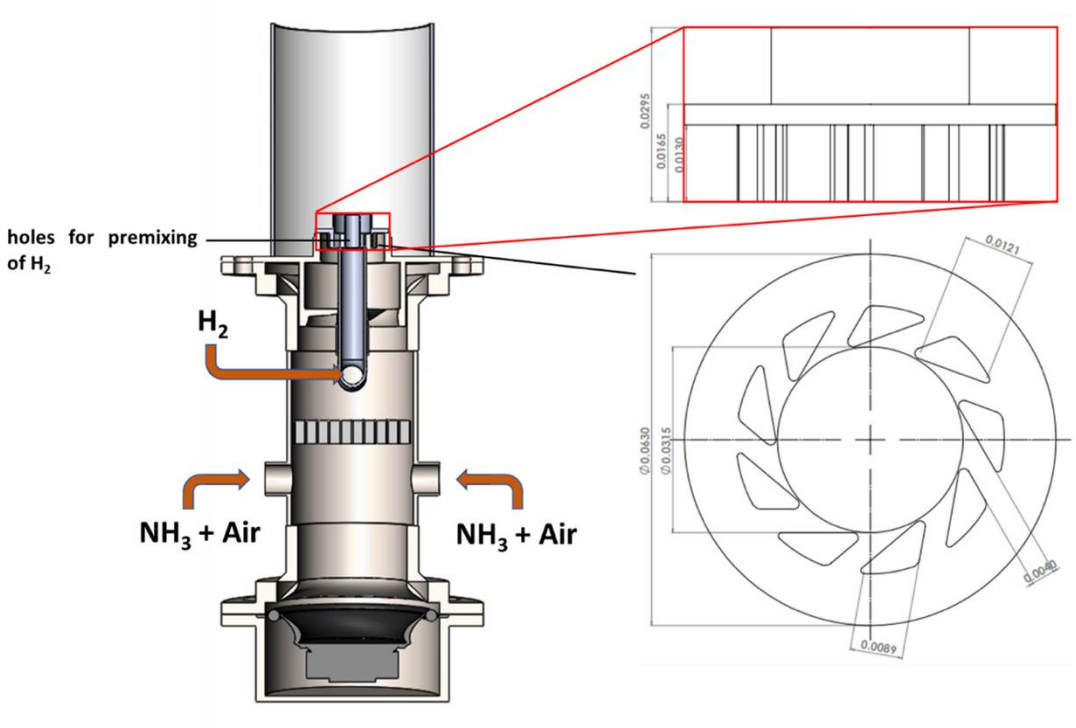

Figure 1: Detailed geometrical view of the burner. Dimensions in meters (m).

A swirl burner with a swirl number, S_g = 1.05 is employed, Figure 1, with a constant thermal power of 8kW and 70/30$_{VOL.\%}$ NH_3/H_2 blend at atmospheric pressure and temperature conditions. Ammonia and air were introduced at the bottom of the mixing chamber, while hydrogen was injected through 6 radially equispaced holes (1.5 mm diameter) at the central lance, located 40 mm below the burner exit, angled at 45˚, directly releasing hydrogen into the swirler to ensure premixing with ammonia and air prior to ignition. Bronkhorst mass flow controllers (±0.5% uncertainty within a range of 15-95% mass flow) were used to control the flow rates of fuel and air. Greater details of the facility can be found in other publications [38], [44],[45].

3. Numerical Methodology

For the complete knowledge of NO_x formation in the current fuel blend of 70% NH_3 + 30% H_2 (by volume), it is important to understand the reaction pathways. The different steps involved in the numerical methodology are explained below.

3.1.Reacting Flow CFD Simulation

This is the first step of numerical evaluation wherein a simplified CFD model/mechanism is employed to get a reacting flow field. To obtain a flame field, first, a 3D non-reacting flow with the appropriate density of inlet streams is simulated. For the 3D simulation, one-third of the burner geometry is simulated with

rotational periodicity. A polygonal mesh of 1.2M elements, which has been validated in the author's previous work [46] is deployed, as shown in Figure 2. Steady RANS simulation is performed with the turbulence modelled using the k-ϵ RNG Model. Pressure and velocity are coupled using the SIMPLEC scheme [47]. The spatial discretisation of all variables is done using the third-order accurate QUICK scheme. The criteria for convergence are selected as 10^{-5} for all residuals.

From the 3D results, the axial, tangential, and radial velocity profiles are extracted. The reacting flow simulations are then performed using a 2D axisymmetric domain with the velocity profiles given as boundary conditions. This is important to ensure the same effect of swirl is reproduced in the 2D axisymmetric domain as it would be observed in the 3D simulation. To establish the credibility of this method, a full 3D combustion is run and compared with the 2D results in Section 5.1 obtained from the above-discussed approach.

Figure 2: Polygonal mesh of 1.2M elements implemented for 3D CFD simulations [38]

For the 2D simulation, a mesh of 0.1M elements is used. For turbulence-chemistry interaction, the Flamelet Generated Manifold is used. Three different reaction mechanisms are considered, i.e. Wang mechanism [40] with 91 species and 444 reactions, Nakamura mechanism [41] with 33 species and 232 reactions, and Glarborg mechanism [42] with 41 species and 270 reactions. The radiation is modelled using the Discrete Ordinate model. The turbulence model, numerical schemes, and convergence criteria are maintained the same as in the 3D cold flow simulations above.

3.2.Chemical Reactor Network

At the core of the CFD-CRN methodology, lies the merging of several CFD elements into a small number of zones that exhibit similar chemical activity and composition. The detailed reaction mechanisms, which are tedious to run for each element of CFD, can be effectively analysed in a few reactors of a CRN. In addition, CRN allows for Rate of Production Analysis, Sensitivity Analysis, Reaction Pathway Analysis, etc., which provide further insights. A CRN consists of idealised reactors like Perfectly Stirred Reactor (PSR) and Plug Flow Reactor (PFR). The PSR is a 0-D reactor, meaning that its parameters, like temperature, species mole fractions, etc., are assumed uniform throughout its volume. The PFR is a 1-D reactor and assumes variation of parameters only in the axial direction but no variation in the cross-stream direction for a given axial position. The construction of CRN is discussed in detail in Section 5.2.

3.3.Quantitative Reaction Pathway Diagrams

From CRN results, the Net Reaction Rates (NRR) for each reaction in the mechanism are obtained. The reactions with a higher magnitude of reaction rate are selected to be plotted in the Quantitative Reaction Pathway Diagram (QRPD). Species relevant to the analysis are selected to be plotted in the QRPD. The species are then connected using arrows as per the selected reactions. The other radical which reacts with the selected species is mentioned in the arrows. The total contribution of reaction rates is summed and a proportional width is assigned to each arrow. This allows for qualitative insights to be drawn from the QRPD.

4. Test Cases

A fuel blend of 70/30 NH_3/H_2 (by volume) is selected for the present study. As discussed in Section 2, the ϕ is varied by controlling the air flow rate, while maintaining the volume flow rates of ammonia and hydrogen at constant values of 11.59 LPM and 27.05 LPM. The volume flow rates of air with the corresponding ϕ are tabulated in Table 1. After studying the experimental results [38], the key points with maximum and minimum NO emission, with the stoichiometric case as a reference were selected for analysis. CRNs were built for four different ϕ (0.65, 0.9, 1.0, and 1.2) based on their respective CFD results. The applicability of each CRN over the range of ϕ, from ϕ = 0.6 to 1.35 is tested. The reason for such extrapolation has been explained in detail in section 5.2.

Table 1: Range of equivalence ratio ϕ and the corresponding volume flow rate of air (in L/min)

ϕ	Air Volume Flow Rate (L/min)
0.60	**207.8**
0.65	**191.8**
0.70	**178.1**
0.75	**166.3**
0.80	**155.9**
0.85	**146.7**
0.90	**138.6**
0.95	**131.3**
1.00	**124.7**
1.05	**118.8**
1.10	**113.4**
1.15	**108.4**

1.20	**103.9**
1.25	**99.8**
1.30	**95.9**
1.35	**92.4**

5. Results & Discussion

In this section, at first, the CFD results and the chemical reactor network (CRN) constructed from it are discussed. Subsequently, the emission results predicted from CRN are compared with the experimental results. Finally, insights into NO_x reaction pathways at different equivalence ratios are compared to understand the dependence of NO_x formation on equivalence ratios.

5.1. CFD Results

The 3D non-reacting simulations are performed first as discussed in Section 3.1 as a precursor to reacting flow simulations. Figure 3a shows streamlines imposed on the time-averaged axial velocity contour on the mid-longitudinal plane obtained from 3D non-reacting simulation for $\phi = 1.2$ – identical fuel-oxidizer flow conditions. The axial, radial, and tangential velocity distributions extracted at the inlet of the combustor (marked as a black dotted line in Figure 3a) are plotted in Figure 3b. These profiles from 3D cold flow simulations are fed as inlet conditions for 2D reacting flow simulations.

The temperature contours with superimposed streamlines from 2D reacting flow simulations using Wang mechanism [40] for $\phi = 1.2$ are shown in Figure 4a. The temperature and species contours resulting from 2D CFD using Nakamura and Glarborg have been omitted for brevity. To verify the applicability of 2D reacting flow simulation using velocity profiles from 3D non-reacting flow for simulating hot flows, the 3D combustion simulation for $\phi = 1.2$ as shown in Figure 4b is also performed and compared with the 2D results. In addition, the overall distribution of the temperature contours also seems comparable. Thus, this establishes a reasonable qualitative agreement between both simulations and hence it is concluded that 2D reacting flow simulations with velocity profiles as inlet conditions from their corresponding 3D non-reacting flow is an economical/simplified way to obtain reacting flow results. This similarity is not unreasonable to expect as reacting and non-reacting flow fields are the same in the flow domain upstream of the combustor exit plane. Further, the validity of 2D CFD is evidenced when the emissions predicted from the CRN built from 2D CFD results are shown to be in good agreement in the later part of this section. The accuracy of CRN produced from 2D reacting flow simulations sharply reduces the computational time required for the CFD simulation by ~55%.

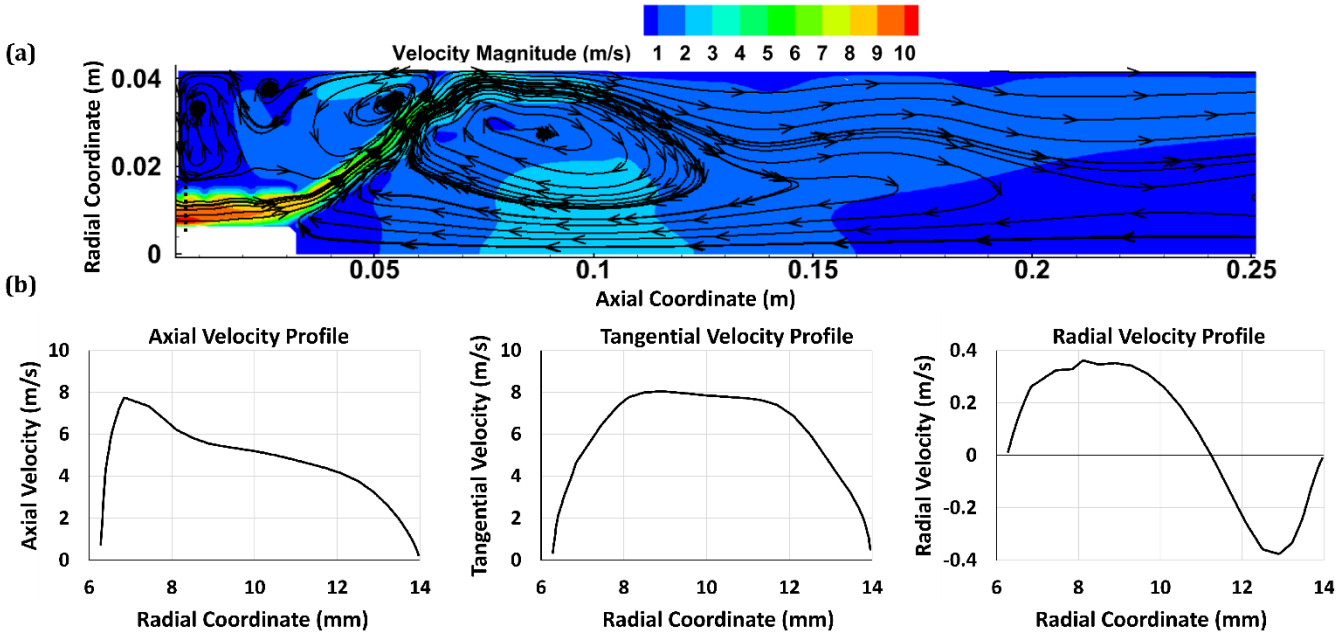

Figure 3: Non-reacting 3D CFD results for ϕ = 1.2. Velocity magnitude contour with imposed streamlines (a). Axial, radial and tangential velocity profiles at the inlet of the combustor from the non-reacting flow field (b).

5.2. Construction of CRN from CFD Results

In Figure 4c, the CFD results for ϕ = 1.2 on the mid-longitudinal plane are analysed and the domain is divided into zones based on velocity field and homogeneity of temperature and species. The procedure used in the construction of CRN at ϕ = 1.2 has been described in detail in this subsection. Of the CRNs constructed with Wang mechanism [40], Nakamura mechanism [41], and Glarborg mechanism [43], each for ϕ = 0.65, 0.9, 1.0, and 1.2, only a single case of ϕ = 1.2 using Wang mechanism [40] has been described in detail, while the rest have been omitted for brevity.

The flame zone, marked by the steep rise in temperature is where the premixed mixture ignites. It is divided into temperature bands of 600 K to 900 K, 900 K to 1200 K, 1200 K to 1500 K, and so on till the highest temperature in the flame zone. The temperature bands are made progressively narrower as the temperature increases because higher reaction rates and gradients of species are expected and zones with smaller temperature variations provide more spatial resolution of the flame. Thus, for ϕ = 1.2, the flame is divided into 7 main zones as 'Mix, F0, F1, F2, F3, F4 and F5'. The seven flame zones are modelled as using a PSR for each zone (thus, 7 PSRs) as shown in Figure 4c. Such methodology has been previously used in [36]. In addition to the flame zones, from the velocity field in Figure 4a, two recirculation zones viz. (a) central toroidal recirculation zone (CTRZ), located at the axis of the burner and (b) Edge Recirculation Zone (ERZ), located between the wall of the burner and the CTRZ are also observed. These zones are defined by negative axial velocity and are characteristic of swirl flows in swirl-stabilized combustors. Both the CTRZ and ERZ are modelled as a PSR as depicted in Figure 4c. Towards the exit of the burner, the streamlines become parallel as flow moves downstream of the CTRZ and the gradients are small in the radial direction. Such a

zone can be regarded as a Post Flame Zone (PFZ) and is modelled as a Plug Flow Reactor (PFR) as shown in Figure 4c.

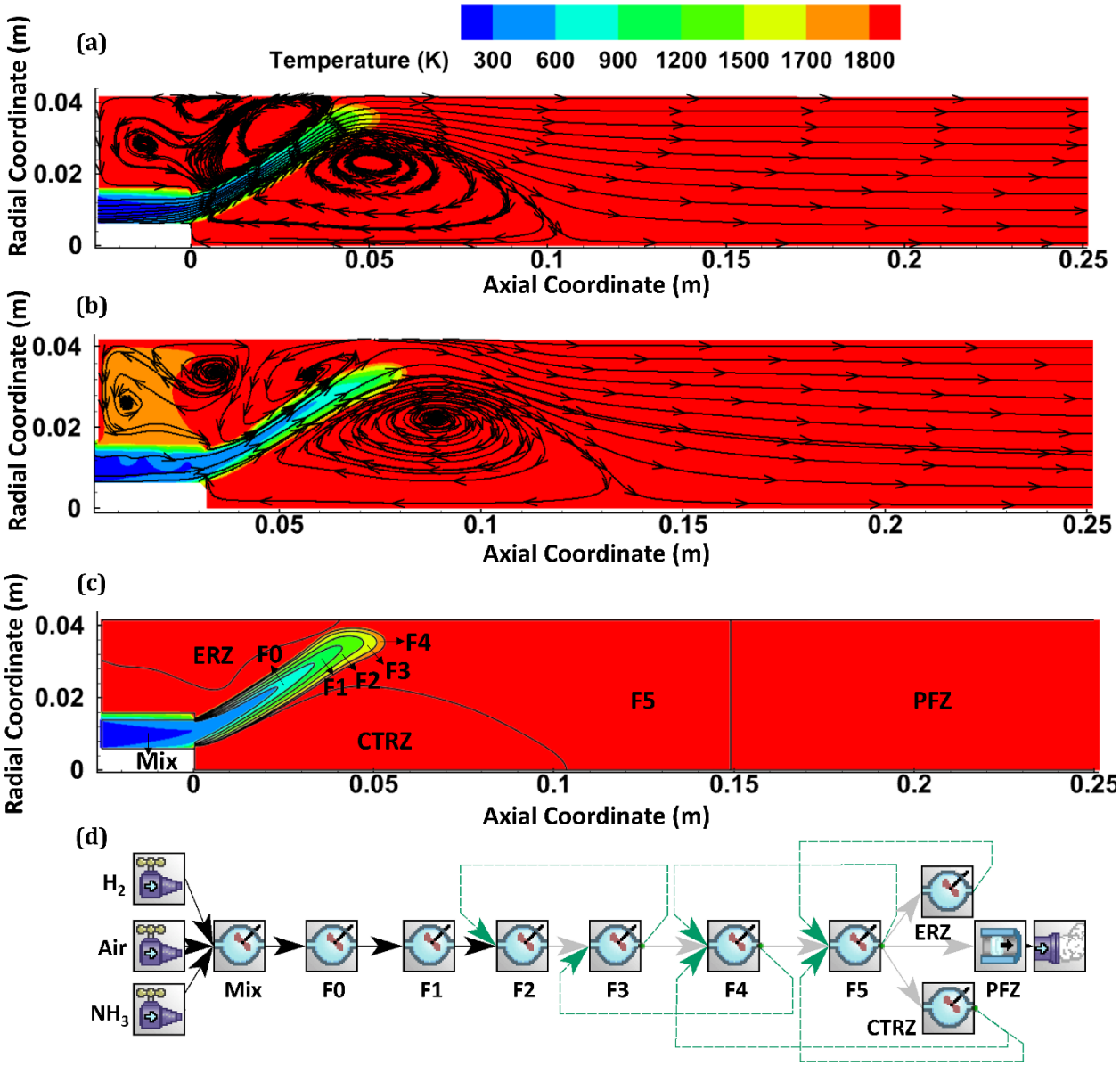

Figure 4: Construction of CRN from CFD results for ϕ = 1.2. Temperature contour with imposed streamlines from 2D reacting flow CFD (a). Temperature contour with imposed streamlines from 3D reacting flow CFD (b). Division of zones for CRN based on temperature and velocity fields (c). Resulting CRN built-in ANSYS Chemkin-Pro (d).

Once the domain has been divided into zones as discussed above, the required inputs to the CRN such as temperature, volume, mass split in between zones, etc., are calculated. The data along the boundary of each zone is extracted and the elemental mass flow rate at each point of the boundary is calculated based on the local density and local velocity field using in-house developed MATLAB code. Such elemental local mass flow rates are integrated as per the requirement to find mass splits accurately between zones. The volume of each zone is calculated using the integration of axisymmetric elemental volume over the entire boundary of that particular zone. The volume-based average temperature is calculated and is given as input to the CRN.

Lastly, the CRN requires a reaction mechanism. As discussed before, Wang mechanism [40], Nakamura mechanism [41], and Glarborg mechanism [42] are employed since these have been proven to be reasonably good mechanisms for a reasonably wide range of equivalence ratios for NH_3-H_2-Air combustion [44]. The entire CRN is implemented using ANSYS Chemkin-Pro 19.2 as shown in Figure 4d.

5.3.CRN Results

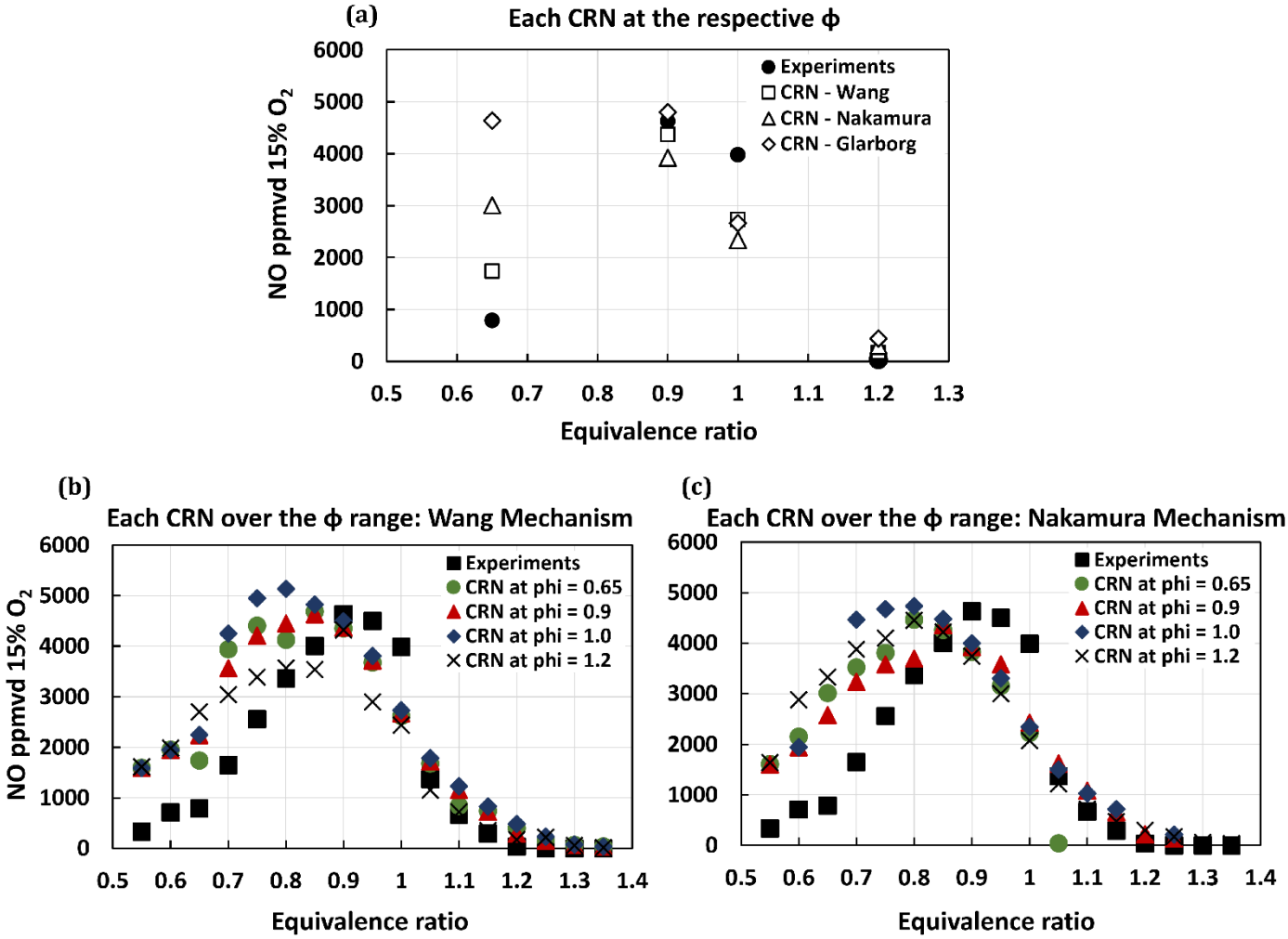

Figure 5: Comparison of the emissions predicted from CFD-CRN methodology with experimental results [38] from respective CRNs (a) and from each CRN run to cover the entire range of ϕ using temperature scaling with Wang mechanism [40] (b) and Nakamura mechanism [41] (c)

Figure 5a depicts the predicted emission of NO from the CRN network from Wang mechanism [40], Nakamura mechanism [41], and Glarborg mechanism [42]. The magnitude of NO at each equivalence ratio (ϕ) is predicted from the CRN corresponding to its ϕ. The predictions are compared with the experimental results [38]. These predictions are in reasonably good agreement with experimental results. In particular, very close values are predicted at ϕ=0.9 and ϕ=1.2 as compared to experiments. While Wang [40] and Nakamura [41] predict close to the experiment, it can be observed that Glarborg [42] despite accurate prediction in the rich, does not satisfactorily predict the pollutants in lean conditions. Although there is some

deviation for Wang [40] and Nakamura [41] mechanisms at ϕ=0.65 and ϕ=1 as compared to the experimental values, it is important to note that the trend of NO as ϕ is varied is correctly predicted by CRN as measured in the experiments. This is a significant milestone because a relatively low-cost CFD-CRN tool described in this work can correctly predict the trend (and at some ϕ, very close values) as compared to expensive experiments which are time-consuming and very difficult to perform. The importance of correctly predicting the trend of NO_x emission by CFD-CRN tool can go a long way in being useful for testing different blends of NH_3-H_2 for different powers (just by knowing the inlet mass flow rates) in a given combustor geometry without performing any experiments. Since Wang [40] and Nakamura [41] mechanisms predicted the NOx emissions reasonably better than Glarborg mechanism [42], the further analyses described here only consider Wang [40] and Nakamura [42] mechanisms.

Upon careful observations in the present study, the inputs to each CRN revealed that the volumes of each respective zone and the mass split from each zone remained almost constant as the ϕ was changed. The only significant difference in the inputs to the CRN was the temperature of each reactor. The highest temperature zones for each ϕ closely resembled the adiabatic flame temperature for the present fuel blend at the respective ϕ. This leads one to conclude that a CRN built for a particular ϕ (using CFD at that ϕ), say at ϕ=0.9, could be used to predict emissions at other ϕ (say, at ϕ=0.65) if the temperature of each zone from CRN at ϕ=0.9 is scaled by a factor so to reasonably predict similar temperature field as at ϕ=0.65. This exercise was performed and to run a CRN over the entire range of ϕ, which was originally based on the results of a specific ϕ, the temperature of each zone is scaled by a factor. This factor is the ratio of the adiabatic flame temperature (AFT) of the target ϕ to that of the original ϕ. The AFT can be calculated without performing tedious simulations. In this way, a CRN built at any ϕ can be used to predict NO emissions at other ϕ. Figure 5b and 5c depicts the NO emission prediction within a range of ϕ=0.55 to 1.35 using CRNs constructed at ϕ=0.65, 0.9, 1, and 1.2 by the method described above, using Wang mechanism [40] and Nakamura mechanism [41] respectively. These mechanisms are chosen based on the accuracy of their NO prediction as seen in Figure 5a. Further, the observation from Figures 5b and 5c, that Wang [40] performs better than Nakamura [41] in rich combustion, is aligned with the findings in one of the author's previous studies.[43] The experimental results depict NO concentration peaking up to 4633 ppmvd 15%O_2 at ϕ = 0.9 which decreases sharply on either side till ϕ = 0.65 and ϕ = 1.2. All four CRNs predict the same trend in close agreement with the experiments.

This is believed to be another significant result. It may not be really necessary to construct CRN by performing CFD at all the ϕ. Instead, one CRN (at any particular ϕ) could be employed to predict the trend of NO at all other ϕ. This could further save computation resources and further simplify the way in which the CFD-CRN tool could be employed in pollutant prediction. It was interesting to introspect the reasons behind the suitability of such a scaling method. It was analyzed that this method of prediction of pollutants

was applicable since all the ϕ had similar flow field characteristics and a reasonable extrapolation of temperature could provide a sufficiently accurate result.

5.4.Analysis of Reaction Pathways

This subsection is dedicated to understanding reaction pathways of NO_x formation at different ϕ. Three ϕ viz. ϕ=0.65 (lean), 0.9 (almost stoichiometric), and 1.2 (slightly rich) are selected in this subsection to identify the difference in NO_x formation pathways.

Figures 6a-6f depict the rates of production (ROP) of NO from various reactions plotted after CRN results using Wang mechanism [40] and Nakamura mechanism [41], (that were validated with the experimental results in the previous subsection). To narrow down the regions of the flame zone that exhibit the highest reactivity, the ROP is compared for various flame zones (i.e., 'Mix, F0, F1, F2, F3, F4, and F5' described previously). It is observed that for ϕ = 0.65 and 0.9, flame zone F3 is the zone with the highest rate of reaction. However, for ϕ = 1.2, F2, F3, and F4 are found to have comparable contributions to the production and/or consumption of NO. Thus, these zones are selected for further analyses for the corresponding ϕ. The post-flame (PFZ) has lower reaction rates compared to the flame zone by, approximately, an order of two and hence, is not considered.

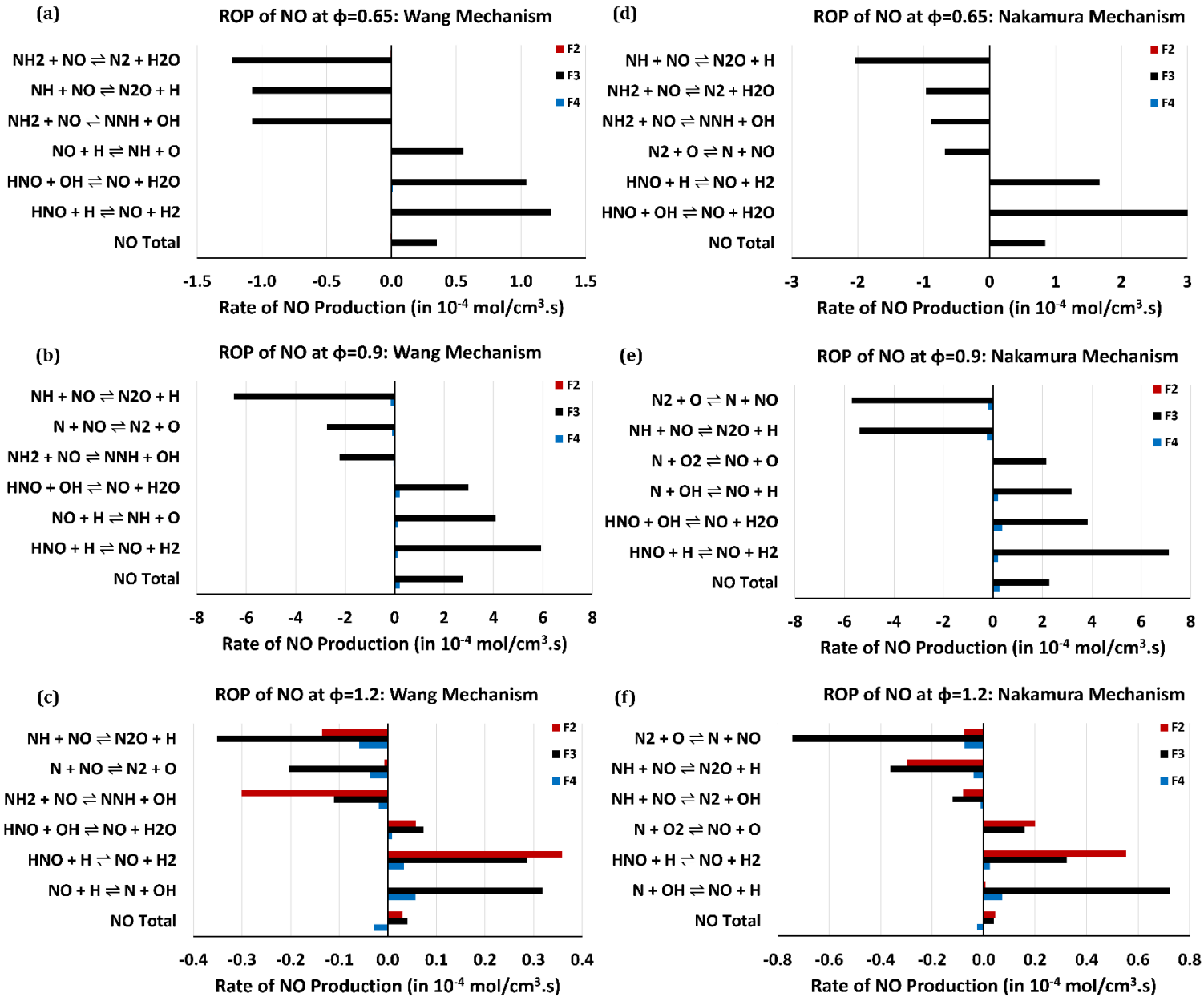

Figure 6: Rates of production of NO from various reactions in the zones of high reactivity at ϕ=0.65 (a), 0.9 (b) and 1.2 (c) using Wang mechanism [40] and at ϕ=0.65 (d), 0.9 (e) and 1.2 (f) using Nakamura mechanism [41].

Based on the reaction rates, quantitative reaction pathway diagrams (QRPD) are constructed using Wang mechanism [40] and Nakamura mechanism [41], for the above-discussed zones for their respective ϕ, as shown in Figures 7a-7f. Based on the QRPDs, the common features from both the above-mentioned mechanisms (in terms of both production and consumption of NO) at ϕ = 0.65, 0.9, and 1.2 are described next. Two pathways for the formation of NO (common to both mechanisms and all ϕ) are found to be as follows:

1. HNO as an H donor: HNO reacts with O, H, OH, NH_2, etc., by donating an H and forming NO along with OH, H_2, H_2O, NH_3, etc. respectively.
2. Oxidation of N/NH: NO is produced when N and NH get oxidized by O_2 in lean combustion. In rich conditions, OH and O respectively oxidise N and NH, leading to NO production.

The relative contribution of these pathways to the net production of NO at different ϕ is shown in Table 2. Both the mechanisms show similar contributions from both pathways at lean conditions, but as ϕ is increased, Nakamura [41] depicts a slower shift from the HNO pathway to the N/NH pathway of NO formation, as compared to Wang [40].

Table 2: Contribution of the NO formation pathways at various ϕ

ϕ	HNO Pathway		N/NH Pathway	
	Wang	Nakamura	Wang	Nakamura
0.65	75%	74%	25%	26%
0.9	55%	65%	45%	35%
1.2	37%	50%	63%	50%

The consumption pathways, common to both Wang [40] and Nakamura [41] mechanisms at all ϕ, of NO reduction pathways using N, NH, and NH_2 are found to be as follows:

1. N + NO Pathway: N reacts with NO to form N_2, which is a desirable product since it is highly stable. Although this pathway is a minor contributor to lean combustion, it gains importance as the combustion becomes rich.
2. NH + NO Pathway: NH reacts with NO to form N_2O majorly and N_2, NNH in the minor. Species like NNH or N_2H_2 eventually form N_2, and hence, do not contribute to NO_x. Although this pathway where N_2 or NNH is produced from NO is a minor contributor in lean combustion, it gains importance as the combustion becomes rich. N_2O production when NO reacts with NH is also the major N_2O formation pathway.
3. NH_2 + NO Pathway: NH_2 reacts with NO to form either N_2 or NNH in comparable amounts. These reactions are more pronounced as the combustion becomes lean.

The table below (Table 3) summarises the radicals, observed from both Wang mechanism [40] and Nakamura mechanism [41], which are involved in the important production and consumption pathways described above:

Table 3: Important reactions in NO_x production and consumption, and the radicals contributing to the reactions.

Reaction name	Reaction	Contributing Radicals
A1	$NH_2 \rightarrow NH$	OH, H
A2	$NH_2 \rightarrow HNO$	O
A3	$NH \rightarrow HNO$	O_2, OH
A4	$NH \rightarrow N$ $NH \rightarrow N_2O$	H, OH NO

A5	$N \rightarrow NO$ $NH \rightarrow NO$	O_2, OH O, O_2
A6	$HNO \rightarrow NO$	H (Also, OH at $\phi = 0.65$)
A7	$N_2O \rightarrow N_2$	H

From the above observations about radicals, it is concluded that OH, O, and H are responsible for most of the oxidation from hydrides of nitrogen to the oxides of nitrogen, which finally amounts to NO_x emissions. At first glance, H being an oxidiser might seem counterintuitive, but the H radical reacts by extracting H to form H_2 and hence, acts as an oxidant.

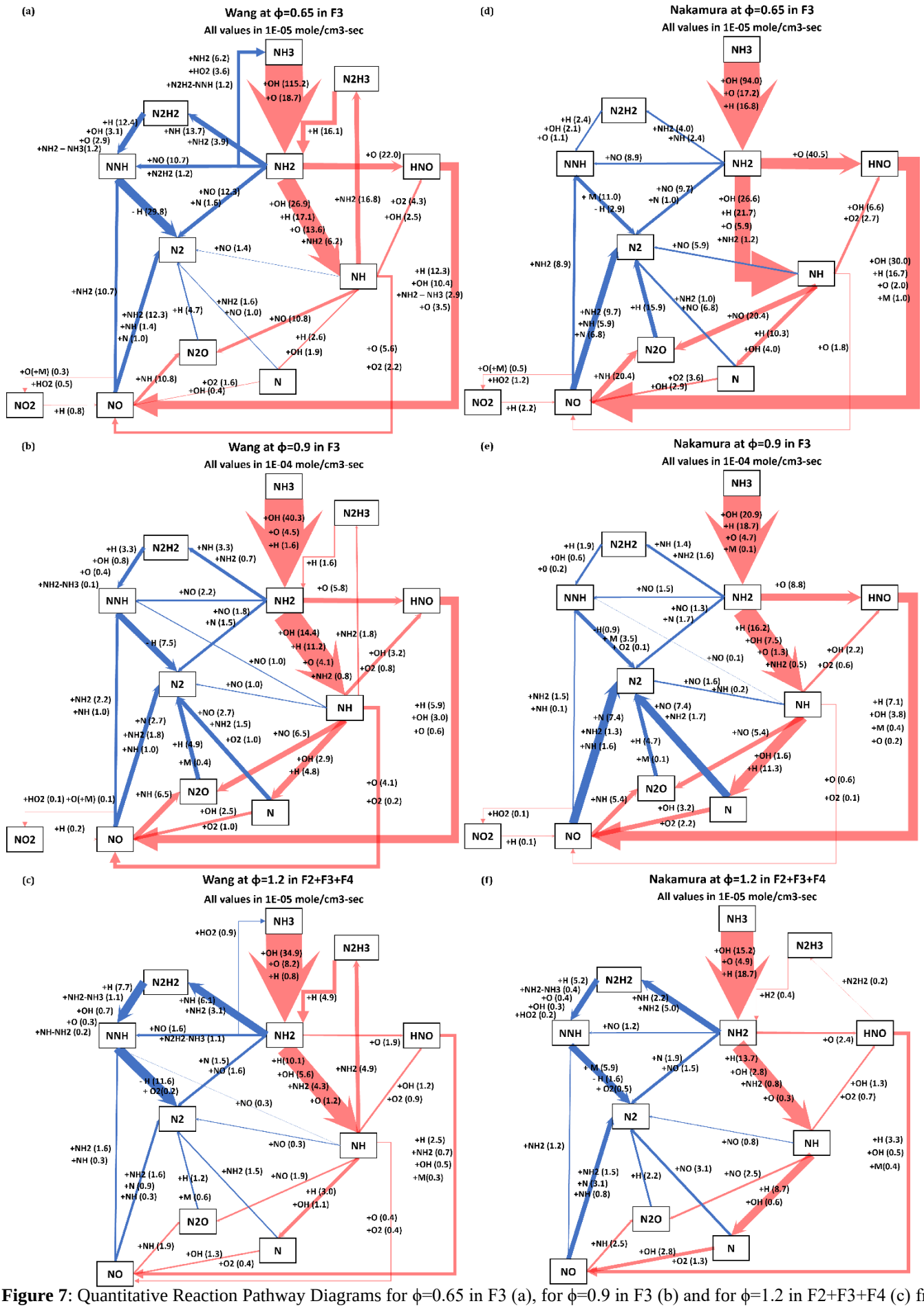

Figure 7: Quantitative Reaction Pathway Diagrams for ϕ=0.65 in F3 (a), for ϕ=0.9 in F3 (b) and for ϕ=1.2 in F2+F3+F4 (c) from Wang mechanism [40] and for ϕ=0.65 in F3 (d), for ϕ=0.9 in F3 (e) and for ϕ=1.2 in F2+F3+F4 (f) from Nakamura mechanism [41].

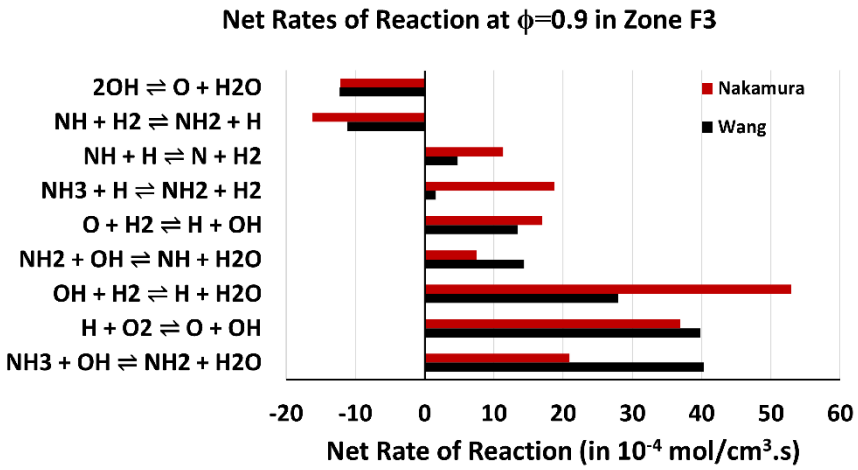

Figure 8: Reactions with the highest net rates of reactions at ϕ=0.9 in zone F3.

The reactions which control OH, O, and H during combustion are identified next. The reactions with the highest net rates of reactions at $\phi = 0.9$ in F3 are shown in Figure 8. It is evident that the same set of reactions is reported to have the highest reaction rates from both mechanisms. At $\phi = 0.65$ and $\phi = 1.2$, the same reactions were observed to have higher net rates of reaction and, thus are not shown here for brevity. The major reactions that contribute to OH, O, and H production are found to be as follows: R1 is the reaction of oxidizer O_2. R2 and R3 are reactions of fuel H_2. R4 is the reaction of dissociation of the product H_2O. The discussion that follows is based on Wang mechanism [40], but since it is fairly qualitative, the same inferences can be drawn by considering the results from Nakamura mechanism [41].

$$\text{R1:} \quad H + O_2 \rightarrow O + OH$$

$$\text{R2:} \quad O + H_2 \rightarrow H + OH$$

$$\text{R3:} \quad OH + H_2 \rightarrow H + H_2O$$

$$\text{R4:} \quad 2OH \rightarrow O + H_2O$$

R1 is found to be one of the reactions with the highest rate of reactions. Almost all of the O_2 from the air undergoes R1 and breaks to form O and OH. In this manner, R1 produces almost all the O and close to half of all the OH during combustion. The R2 and R3 produce the majority of H from the reactant H_2. These two reactions neither produce nor consume much OH, because OH is a reactant (in R3) as well as a product (in R2). The R4 has a significant negative rate of reaction and produces the other half of the OH during combustion, by breaking of product H_2O.

In the case of lean combustion, there is an abundance of O_2 and a scarcity of H_2. Due to scarce H_2, the reactions R2 and R3 are inhibited as they depend on H_2 as a reactant. Since, as discussed in the previous paragraph, R2, and R3 produce almost all the H, there is a scarcity of H as well. Further due to inhibition of R3, there is lesser H_2O which further inhibits R4. A decrease in R4 causes a decrease in the availability of OH. Similar to the above discussion, in the case of rich combustion, there is an abundance of H_2 and a scarcity

of O_2. Due to scarce O2, R1 is inhibited as it requires O_2 as a reactant. Since R1 produces almost all the O, there is a scarcity of O as well. Further, due to the unavailability of O, R4 is inhibited, causing a decrease in the availability of OH. Due to these reasons, the production of OH will be favoured close to stoichiometric instead of rich or lean combustion. This discussion has been presented diagrammatically in Figure 9.

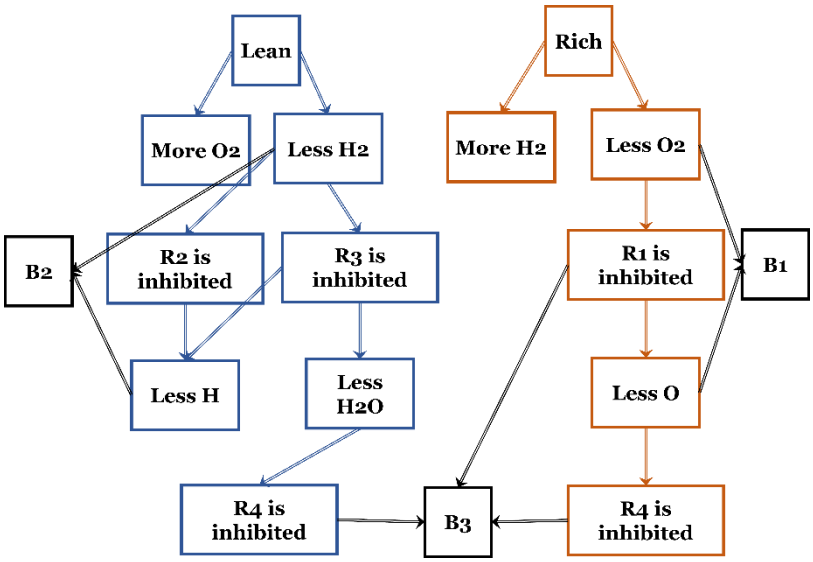

Figure 9: The effect of stoichiometry on the availability of OH, O, and H radicals

Based on the above discussion the following conclusions are drawn:

B1. All the reactions which depend on O or O_2 will be impeded in the case of rich combustion and favoured in the case of lean combustion.

B2. All the reactions which depend on H or H_2 will be impeded in the case of lean combustion and favoured in the case of rich combustion.

B3. All the reactions which depend on OH will be impeded in the case of both rich or lean combustion and favoured close to stoichiometric combustion.

With the above discussion as the background, next, the variation in NO production at the three chosen ϕ = 0.65, 0.9, and 1.2 is discussed along with possible reasons.

In order to explain the differences in NO production at the three chosen ϕ = 0.65, 0.9, and 1.2, the important radicals that cause the differences are identified. Then, these radicals are shown to be controlled by the ϕ, thus describing how NO emissions are innately linked with the stoichiometry of the combustion.

The reaction pathways of NO formation (resulting in variation of NO production) vary with ϕ as follows:

C1. NH_2 forms more NH, HNO, and lesser NNH, N_2H_2, and N_2 at ϕ = 0.9 (compared to 0.65 or 1.2). As more NH and HNO favour more NO (as described previously as two formation pathways), the NO emission peaks at 0.9. This shift can be observed qualitatively from the QRPDs by comparing the

thickness of blue arrows going to the left from NH_2 to the thickness of the red arrows going to the right from NH_2.

C2. NH_2 forms more NH and less HNO as the combustion becomes rich. This establishes the governing pathways of NO_x emission at different ϕ. This shift can be observed qualitatively from the QRPDs by comparing the thickness of the arrows towards NO via HNO and the thickness of the arrows towards NO via N/NH.

C3. NH forms more N_2O and less N as the combustion becomes lean. Due to this, a rise in N_2O is observed at lean combustion. This shift can be observed qualitatively from the QRPDs by comparing the thickness of the arrows from NH going towards N_2O and the thickness of the arrows from NH going towards N.

The explanation for these shifts in reaction pathways is as follows:

Explanation of C1: The radical OH is found to be responsible for driving forward the reactions from NH_2 to NH to HNO (refer to A1, A3, and A4 in Table 3). This further implies that OH promotes the formation of NH, and HNO from NH_2 instead of the formation of NNH, N_2H_2, and N_2. The high amount of OH close to stoichiometric (refer to B3), thus elevates NO emission by reducing NNH, N_2H_2, etc., which eventually results in stable product N_2. Additionally, in lean combustion, NH_2 forms less NH (refer to A1 and B2) while in rich combustion, NH_2 forms less HNO (refer to A2 and B1). This further promotes NH_2 to form N_2, N_2H_2, or NNH in the case of lean as well as rich cases. C1 along with C2 explains why the peak of NO occurs close to stoichiometric.

Explanation of C2: In lean combustion, the dominant pathway of NO formation is the HNO pathway. Since the formation of HNO from NH_2 (refer to A2) or NH (refer to A3) is controlled by O and O_2, this pathway is promoted in the lean regime (refer to B1). In rich combustion, N/NH oxidation becomes the dominant pathway as the formation of N and NH from NH_2 (refer to A1 and A4) is promoted because it is controlled by H (refer to B2).

It should be noted that neither of these pathways is solely dependent on just one radical O or H. For example, in lean combustion, although the ease of HNO formation is higher, the conversion of HNO to NO (refer to A6) is difficult since it is majorly controlled by H (refer to B2). Similarly in rich combustion, although the ease of NH and N formation is higher, the conversion of NH or N to NO (refer to A5) is difficult since it is majorly controlled by O_2 and O (refer to B1). These countermeasures in each pathway obstruct high NO production in lean and rich conditions. In this manner, the explanation of C1 and C2 presents a complete explanation as to why the NO emissions peak close to stoichiometric combustion.

Explanation of C3: In lean combustion, the conversion of NH to N (refer to A4) is suppressed because it is controlled by H (refer to B2) and this allows for the availability of NH to form N_2O. There is an availability

of NO formed via the HNO pathway in lean combustion. Due to this, the reactants required for N_2O production via the reaction NH + NO → N_2O + H are present sufficiently. This reaction is the prime N_2O-producing pathway. Furthermore, in lean combustion, the consumption of N_2O to form N_2 (refer to A7) is also suppressed because it is controlled by H (refer to B2). These factors contribute to the peaking of N_2O as the combustion becomes lean.

In the above discussion, stoichiometric combustion is pointed out to produce the highest NO. However, the results of NO emission show the peak to occur at $\phi = 0.9$ instead of $\phi = 1.0$. If looked at closely, there are many reactions with H as an oxidant where H_2 is formed in the products. It is due to this reformation of fuel that a slightly lean mixture is needed to consume all the fuel and hence, the peak of NO shifts towards the lean.

The variation of emission pathways as ϕ is varied, based on the effect of OH, H, and O radicals is summarised in Figure 10. The reactions which are promoted by a radical are shown in solid arrows while the reactions which are impeded by a radical are shown in dashed arrows. Figure 10a shows strong N_2O-producing pathways but weak N_2O-consuming pathways, leading to the peak in N_2O. Figure 10b graphically represents the continuous pathway of solid black arrows for the formation of NO at $\phi = 0.9$, leading to the peak of NO close to stoichiometric. Figures 10a and 10c represent the dominant NO-producing pathway for lean and rich combustion respectively.

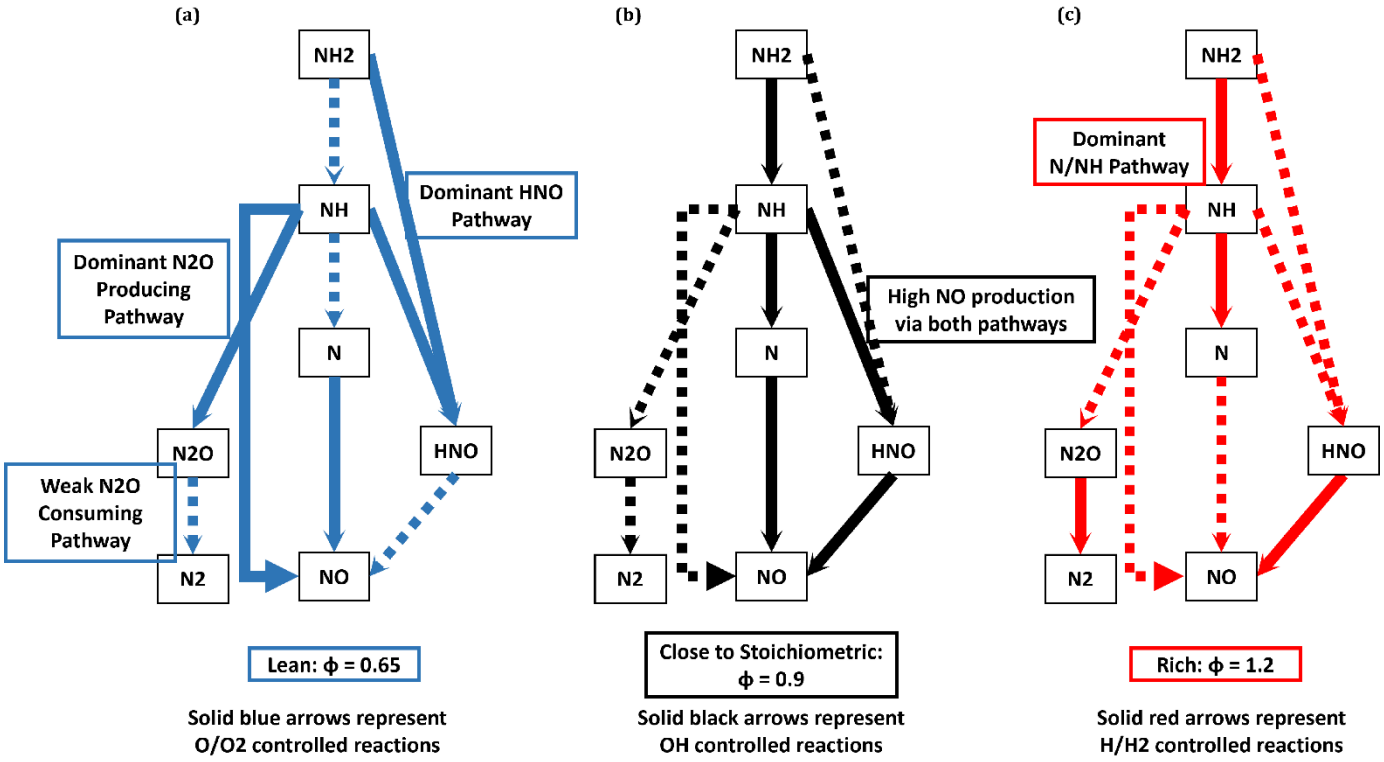

Figure 10: Summary of the reaction pathways at $\phi = 0.65$ (a), 0.9 (b) and 1.2 (c)

6. Conclusion

In this study, the NO_x emission characteristics of 70/30 Ammonia – Hydrogen (by volume) premixed combustion have been studied. Chemical reactor networks (CRN) based on CFD simulations have been implemented and NO emission results from Wang mechanism [40], Nakamura mechanism [41], and Glarborg mechanism [42] have been compared to experimental results. Due to better prediction of NO emissions, especially in lean combustion, Wang [40] and Nakamura [41] mechanisms were considered for further probing. Both the mechanisms agreed upon the qualitative explanation for how stoichiometry controls the pathways and emissions, still there were slight deviations in their prediction of the relative contribution of pathways at various ϕ.

Rates of Production and Quantitative Reaction Pathway Diagrams have been studied to explain the experimental trends in pollutants and the shifting in reaction pathways. The findings have been summarised as the following:

1. The NO formation pathways were found to lie in either of two classes, via HNO as an H donor or Oxidation of N/NH. NO consumption pathways included the reduction of NO via N, NH or NH_2. The $NO + NH \rightarrow N_2O + H$ pathway was also found to be the chief N_2O-producing pathway.
2. The peak in NO close to stoichiometric combustion was found to be due to higher OH availability compared to lean or rich conditions. Further, neither of the NO formation pathways is solely dependent upon H or O and hence are hindered in the case of lean and rich combustion respectively.
3. The HNO as an H donor pathway is dominant in lean combustion. This is because the formation of HNO from NH_2 or NH is dependent on O and O_2 respectively. As a result, as combustion becomes rich, the oxidation of the N/NH pathway of NO formation becomes important.
4. In lean conditions, due to the unavailability of H, it is unfavourable for NH to form N. Due to this, NH is available to react with NO to produce N_2O. This explains two important experimental observations, vis, an increase in N_2O and a decrease in NO in the case of lean combustion.
5. The shifting of the NO peak to slightly lean combustion can be accounted for by the strong oxidant species H, which reacts to extract H and forms H_2. The extra H_2 requires more air in order to effectively set up stoichiometric combustion.

Acknowledgements

The IIT (BHU) Varanasi authors acknowledge the funding received by SERB, India (Grant No: SRG/2022/000518) for this work. Cardiff University authors gratefully acknowledge the support from the ESPRC through the program SAFE AGT (EP/T009314/1) and Optimal fuel blends for ammonia-fueled thermal propulsion systems (EP/T033800/1). Information on the data underpinning the results presented here, including how to access them, can be found in the Cardiff University data catalogue at http://orca.cf.ac.uk/XXXXX. The authors would like to thank Dr. Joanna Jójka (Poznan University of Technology, Poznan, Poland) and Ali Alnasif (Cardiff University, Cardiff, UK) for their help in running numerical simulations.

References

1. Kobayashi, Hideaki, Akihiro Hayakawa, K.D. Kunkuma A. Somarathne, and Ekenechukwu C. Okafor. “Science and Technology of Ammonia Combustion.” Proceedings of the Combustion Institute 37, no. 1 (2019): 109–33. https://doi.org/10.1016/j.proci.2018.09.029.
2. Morlanés, Natalia, Sai P. Katikaneni, Stephen N. Paglieri, Aadesh Harale, Bandar Solami, S. Mani Sarathy, and Jorge Gascon. “A Technological Roadmap to the Ammonia Energy Economy: Current State and Missing Technologies.” Chemical Engineering Journal 408 (March 2021): 127310. https://doi.org/10.1016/j.cej.2020.127310.
3. Valera-Medina, A, H Xiao, M Owen-Jones, W.I.F. David, and P.J. Bowen. “Ammonia for Power.” Progress in Energy and Combustion Science 69 (November 2018): 63–102. https://doi.org/10.1016/j.pecs.2018.07.001.
4. Cardoso, João Sousa, Valter Silva, Rodolfo C. Rocha, Matthew J. Hall, Mário Costa, and Daniela Eusébio. “Ammonia as an Energy Vector: Current and Future Prospects for Low-Carbon Fuel Applications in Internal Combustion Engines.” Journal of Cleaner Production 296 (May 2021): 126562. https://doi.org/10.1016/j.jclepro.2021.126562.
5. Xu, Xianxian, Quan Zhou, and Dehai Yu. “The Future of Hydrogen Energy: Bio-Hydrogen Production Technology.” International Journal of Hydrogen Energy 47, no. 79 (September 2022): 33677–98. https://doi.org/10.1016/j.ijhydene.2022.07.261.
6. Brandon, N. P., and Z. Kurban. “Clean Energy and the Hydrogen Economy.” Philosophical Transactions of the Royal Society A: Mathematical, Physical and Engineering Sciences 375, no. 2098 (July 28, 2017): 20160400. https://doi.org/10.1098/rsta.2016.0400.
7. Bossel, Ulf, and Baldur Eliasson. "Energy and the hydrogen economy." Methanol Institute, Arlington, VA (2003).
8. Chiuta, Steven, Raymond C. Everson, Hein W.J.P. Neomagus, Percy Van Der Gryp, and Dmitri G. Bessarabov. “Reactor Technology Options for Distributed Hydrogen Generation via Ammonia Decomposition: A Review.” International Journal of Hydrogen Energy 38, no. 35 (November 2013): 14968–91. https://doi.org/10.1016/j.ijhydene.2013.09.067.
9. Elbaz, Ayman M., Shixing Wang, Thibault F. Guiberti, and William L. Roberts. “Review on the Recent Advances on Ammonia Combustion from the Fundamentals to the Applications.” Fuel Communications 10 (March 2022): 100053. https://doi.org/10.1016/j.jfueco.2022.100053.
10. Langella, G., M. de Joannon, P. Sabia, P. Iodice, and A. Amoresano. "Ammonia as a fuel for internal combustion engines: latest advances and future challenges." In Journal of Physics: Conference Series, vol. 2385, no. 1, p. 012036. IOP Publishing, 2022.
11. Feibelman, Peter J., and Roland Stumpf. "Comments on potential roles of ammonia in a hydrogen economy—a study of issues related to the use of ammonia for on-board vehicular hydrogen storage." Sandia Natl. Lab (2006).
12. Gray Jr, James T., Edward Dimitroff, Nelson T. Meckel, and R. D. Quillian Jr. "Ammonia fuel—engine compatibility and combustion." SAE Transactions (1967): 785-807.
13. Kurata, Osamu, Norihiko Iki, Takayuki Matsunuma, Takahiro Inoue, Taku Tsujimura, Hirohide Furutani, Hideaki Kobayashi, and Akihiro Hayakawa. “Performances and Emission Characteristics of NH3–Air and NH3CH4–Air Combustion Gas-Turbine Power Generations.” Proceedings of the Combustion Institute 36, no. 3 (2017): 3351–59. https://doi.org/10.1016/j.proci.2016.07.088.
14. Ichikawa, Akinori, Akihiro Hayakawa, Yuichi Kitagawa, K.D. Kunkuma Amila Somarathne, Taku Kudo, and Hideaki Kobayashi. “Laminar Burning Velocity and Markstein Length of Ammonia/Hydrogen/Air Premixed Flames at Elevated Pressures.” International Journal of Hydrogen Energy 40, no. 30 (August 2015): 9570–78. https://doi.org/10.1016/j.ijhydene.2015.04.024.

15. Valera-Medina, A., D.G. Pugh, P. Marsh, G. Bulat, and P. Bowen. “Preliminary Study on Lean Premixed Combustion of Ammonia-Hydrogen for Swirling Gas Turbine Combustors.” International Journal of Hydrogen Energy 42, no. 38 (September 2017): 24495–503. https://doi.org/10.1016/j.ijhydene.2017.08.028.
16. Li, Jun, Hongyu Huang, Noriyuki Kobayashi, Zhaohong He, and Yoshihiro Nagai. “Study on Using Hydrogen and Ammonia as Fuels: Combustion Characteristics and NO x Formation: Hydrogen and Ammonia as Fuels.” International Journal of Energy Research 38, no. 9 (July 2014): 1214–23. https://doi.org/10.1002/er.3141.
17. Valera-Medina, A., M. Gutesa, H. Xiao, D. Pugh, A. Giles, B. Goktepe, R. Marsh, and P. Bowen. “Premixed Ammonia/Hydrogen Swirl Combustion under Rich Fuel Conditions for Gas Turbines Operation.” International Journal of Hydrogen Energy 44, no. 16 (March 2019): 8615–26. https://doi.org/10.1016/j.ijhydene.2019.02.041.
18. Mei, Bowen, Jianguo Zhang, Xiaoxiang Shi, Zhongya Xi, and Yuyang Li. “Enhancement of Ammonia Combustion with Partial Fuel Cracking Strategy: Laminar Flame Propagation and Kinetic Modeling Investigation of NH3/H2/N2/Air Mixtures up to 10 Atm.” Combustion and Flame 231 (September 2021): 111472. https://doi.org/10.1016/j.combustflame.2021.111472.
19. Hayakawa, Akihiro, Takashi Goto, Rentaro Mimoto, Yoshiyuki Arakawa, Taku Kudo, and Hideaki Kobayashi. “Laminar Burning Velocity and Markstein Length of Ammonia/Air Premixed Flames at Various Pressures.” Fuel 159 (November 2015): 98–106. https://doi.org/10.1016/j.fuel.2015.06.070.
20. Hayakawa, Akihiro, Takashi Goto, Rentaro Mimoto, Taku Kudo, and Hideaki Kobayashi. “NO Formation/Reduction Mechanisms of Ammonia/Air Premixed Flames at Various Equivalence Ratios and Pressures.” Mechanical Engineering Journal 2, no. 1 (2015): 14-00402-14–00402. https://doi.org/10.1299/mej.14-00402.
21. Lindstedt, R. P., F. C. Lockwood, and M. A. Selim. “Detailed Kinetic Modelling of Chemistry and Temperature Effects on Ammonia Oxidation.” Combustion Science and Technology 99, no. 4–6 (September 1994): 253–76. https://doi.org/10.1080/00102209408935436.
22. Skreiberg, Øyvind, Pia Kilpinen, and Peter Glarborg. “Ammonia Chemistry below 1400 K under Fuel-Rich Conditions in a Flow Reactor.” Combustion and Flame 136, no. 4 (March 2004): 501–18. https://doi.org/10.1016/j.combustflame.2003.12.008.
23. Tian, Zhenyu, Yuyang Li, Lidong Zhang, Peter Glarborg, and Fei Qi. “An Experimental and Kinetic Modeling Study of Premixed NH3/CH4/O2/Ar Flames at Low Pressure.” Combustion and Flame 156, no. 7 (July 2009): 1413–26. https://doi.org/10.1016/j.combustflame.2009.03.005.
24. Duynslaegher, C., H. Jeanmart, and J. Vandooren. “Ammonia Combustion at Elevated Pressure and Temperature Conditions.” Fuel 89, no. 11 (November 2010): 3540–45. https://doi.org/10.1016/j.fuel.2010.06.008.
25. Song, Yu, Hamid Hashemi, Jakob Munkholt Christensen, Chun Zou, Paul Marshall, and Peter Glarborg. “Ammonia Oxidation at High Pressure and Intermediate Temperatures.” Fuel 181 (October 2016): 358–65. https://doi.org/10.1016/j.fuel.2016.04.100.
26. Otomo, Junichiro, Mitsuo Koshi, Teruo Mitsumori, Hiroshi Iwasaki, and Koichi Yamada. “Chemical Kinetic Modeling of Ammonia Oxidation with Improved Reaction Mechanism for Ammonia/Air and Ammonia/Hydrogen/Air Combustion.” International Journal of Hydrogen Energy 43, no. 5 (February 1, 2018): 3004–14. https://doi.org/10.1016/j.ijhydene.2017.12.066.
27. Kobayashi, Hideaki, Akihiro Hayakawa, K.D. Kunkuma A. Somarathne, and Ekenechukwu C. Okafor. “Science and Technology of Ammonia Combustion.” Proceedings of the Combustion Institute 37, no. 1 (2019): 109–33. https://doi.org/10.1016/j.proci.2018.09.029.

28. Sturgess, G., and D. Shouse. “A Hybrid Model for Calculating Lean Blowouts in Practical Combustors.” In 32nd Joint Propulsion Conference and Exhibit. Lake Buena Vista,FL,U.S.A.: American Institute of Aeronautics and Astronautics, 1996. https://doi.org/10.2514/6.1996-3125.
29. Benedetto, D., S. Pasini, M. Falcitelli, C. La Marca, and L. Tognotti. “NO X Emission Prediction from 3-D Complete Modelling to Reactor Network Analysis.” Combustion Science and Technology 153, no. 1 (April 2000): 279–94. https://doi.org/10.1080/00102200008947265.
30. Benedetto, Davide, Sauro Pasini, Mariano Falcitelli, Cristiana La Marca, and Leonardo Tognotti. “Predicting Pollutant Emissions from Combustion Systems Using a Novel Integrated Methodology.” Progress in Computational Fluid Dynamics, An International Journal 1, no. 1/2/3 (2001): 50. https://doi.org/10.1504/PCFD.2001.001470.
31. Faravelli, T., L. Bua, A. Frassoldati, A Antifora, L. Tognotti, and E. Ranzi. “A New Procedure for Predicting NO_x Emissions from Furnaces.” Computers & Chemical Engineering 25, no. 4–6 (May 2001): 613–18. https://doi.org/10.1016/S0098-1354(01)00641-X.
32. Falcitelli, M., S. Pasini, N. Rossi, and L. Tognotti. “CFD+reactor Network Analysis: An Integrated Methodology for the Modeling and Optimisation of Industrial Systems for Energy Saving and Pollution Reduction.” Applied Thermal Engineering 22, no. 8 (June 2002): 971–79. https://doi.org/10.1016/S1359-4311(02)00014-5.
33. Novosselov, I. V., P. C. Malte, S. Yuan, R. Srinivasan, and J. C. Y. Lee. “Chemical Reactor Network Application to Emissions Prediction for Industrial DLE Gas Turbine.” In Volume 1: Combustion and Fuels, Education, 221–35. Barcelona, Spain: ASMEDC, 2006. https://doi.org/10.1115/GT2006-90282.
34. Lebedev, A.B., A.N. Secundov, A.M. Starik, N.S. Titova, and A.M. Schepin. “Modeling Study of Gas-Turbine Combustor Emission.” Proceedings of the Combustion Institute 32, no. 2 (2009): 2941–47. https://doi.org/10.1016/j.proci.2008.05.015.
35. Park, Jungkyu, Truc Huu Nguyen, Daero Joung, Kang Yul Huh, and Min Chul Lee. “Prediction of NO x and CO Emissions from an Industrial Lean-Premixed Gas Turbine Combustor Using a Chemical Reactor Network Model.” Energy & Fuels 27, no. 3 (March 21, 2013): 1643–51. https://doi.org/10.1021/ef301741t.
36. Nguyen, Truc Huu, Seunghan Kim, Jungkyu Park, Seungchai Jung, and Shaun Kim. “CFD-CRN Validation Study for NO_x Emission Prediction in Lean Premixed Gas Turbine Combustor.” Journal of Mechanical Science and Technology 31, no. 10 (October 2017): 4933–42. https://doi.org/10.1007/s12206-017-0942-2.
37. Yousefian, Sajjad, Gilles Bourque, and Rory F. D. Monaghan. “Review of Hybrid Emissions Prediction Tools and Uncertainty Quantification Methods for Gas Turbine Combustion Systems.” In Volume 4B: Combustion, Fuels and Emissions, V04BT04A005. Charlotte, North Carolina, USA: American Society of Mechanical Engineers, 2017. https://doi.org/10.1115/GT2017-64271.
38. Mashruk, S., S.E. Zitouni, P. Brequigny, C. Mounaim-Rousselle, and A. Valera-Medina. “Combustion Performances of Premixed Ammonia/Hydrogen/Air Laminar and Swirling Flames for a Wide Range of Equivalence Ratios.” International Journal of Hydrogen Energy 47, no. 97 (December 2022): 41170–82. https://doi.org/10.1016/j.ijhydene.2022.09.165.
39. Verkamp, F.J., M.C. Hardin, and J.R. Williams. “Ammonia Combustion Properties and Performance in Gas-Turbine Burners.” Symposium (International) on Combustion 11, no. 1 (January 1967): 985–92. https://doi.org/10.1016/S0082-0784(67)80225-X.
40. Wang, Zhihua, Xinlu Han, Yong He, Runfan Zhu, Yanqun Zhu, Zhijun Zhou, and Kefa Cen. “Experimental and Kinetic Study on the Laminar Burning Velocities of NH3 Mixing with CH3OH and C2H5OH in Premixed Flames.” Combustion and Flame 229 (July 2021): 111392. https://doi.org/10.1016/j.combustflame.2021.02.038.

41. Nakamura, Hisashi, Susumu Hasegawa, and Takuya Tezuka. “Kinetic Modeling of Ammonia/Air Weak Flames in a Micro Flow Reactor with a Controlled Temperature Profile.” Combustion and Flame 185 (November 2017): 16–27. https://doi.org/10.1016/j.combustflame.2017.06.021.
42. Glarborg, Peter. “The NH 3 /NO 2 /O 2 System: Constraining Key Steps in Ammonia Ignition and N 2 O Formation.” Combustion and Flame, August 2022, 112311. https://doi.org/10.1016/j.combustflame.2022.112311.
43. Alnasif, Ali, Syed Mashruk, Masao Hayashi, Joanna Jójka, Hao Shi, Akihiro Hayakawa, and Agustin Valera-Medina. Performance Investigation of Currently Available Reaction Mechanisms in the Estimation of NO Measurements: A Comparative Study.” Energies 16, no. 9 (April 29, 2023): 3847. https://doi.org/10.3390/en16093847.
44. Mashruk, Syed, Marina Kovaleva, Ali Alnasif, Cheng Tung Chong, Akihiro Hayakawa, Ekenechukwu C. Okafor, and Agustin Valera-Medina. “Nitrogen Oxide Emissions Analyses in Ammonia/Hydrogen/Air Premixed Swirling Flames.” Energy 260 (December 2022): 125183. https://doi.org/10.1016/j.energy.2022.125183.
45. Mashruk, S., E.C. Okafor, M. Kovaleva, A. Alnasif, D. Pugh, A. Hayakawa, and A. Valera-Medina. “Evolution of N2O Production at Lean Combustion Condition in NH3/H2/Air Premixed Swirling Flames.” Combustion and Flame 244 (October 2022): 112299. https://doi.org/10.1016/j.combustflame.2022.112299.
46. Mashruk, Syed, Hua Xiao, Daniel Pugh, Meng-Choung Chiong, Jon Runyon, Burak Goktepe, Anthony Giles, and Agustin Valera-Medina. “Numerical Analysis on the Evolution of NH2 in Ammonia/Hydrogen Swirling Flames and Detailed Sensitivity Analysis under Elevated Conditions.” Combustion Science and Technology 195, no. 6 (April 26, 2023): 1251–78. https://doi.org/10.1080/00102202.2021.1990897.
47. Jang, D. S., R. Jetli, and S. Acharya. “COMPARISON OF THE PISO, SIMPLER, AND SIMPLEC ALGORITHMS FOR THE TREATMENT OF THE PRESSURE-VELOCITY COUPLING IN STEADY FLOW PROBLEMS.” Numerical Heat Transfer 10, no. 3 (September 1986): 209–28. https://doi.org/10.1080/10407788608913517.